



Permittivity and modulus spectroscopic study of $\text{BaFe}_{0.5}\text{Nb}_{0.5}\text{O}_3$ ceramics

Subrat K. Kar, Pawan Kumar*

Department of Physics, National Institute of Technology, Rourkela 769008, India

Received 26 September 2013; received in revised form 23 December 2013; accepted 25 December 2013

Abstract

$\text{Ba}(\text{Fe}_{0.5}\text{Nb}_{0.5})\text{O}_3$ (BFN) powder was synthesized in single perovskite phase by conventional solid state reaction route and BFN ceramic was obtained by uniaxial pressing and sintering at 1350 °C. Complex immittance like: permittivity and modulus spectroscopic formalism were simultaneously used to explain dielectric behaviour of the ceramics. The activation energy calculated from dielectric relaxation below 100 °C was found to be ~ 0.19 eV. The activation energy obtained from modulus spectra above 100 °C was ~ 0.59 eV. The space charge polarization model was used to explain the origin of relaxation and “giant” permittivity of BFN ceramics near room temperature.

Keywords: perovskites, sintering, electrical properties, impedance spectroscopy, capacitors

I. Introduction

Global trends in miniaturization in electronic devices and components prompted the ceramic and electronic industries to search for high dielectric constant materials. Memory devices such as static and dynamic random access memories are based on high capacitance materials and the degree of miniaturization depends on the static dielectric constant ϵ' of a material. In addition to memory applications, high dielectric constant materials are also widely used in multilayer capacitor (MLC) and microelectronic devices [1,2]. Ferroelectric materials show high dielectric constants, but with certain limitations: i) value of ϵ' is high only near the Curie transition temperature, T_c , ii) there is a large variation of ϵ' near T_c , iii) less temperature stability of ϵ' , iv) high ϵ' is possessed by lead based ferroelectric materials, which are toxic in nature.

$\text{Ba}(\text{Fe}_{0.5}\text{Nb}_{0.5})\text{O}_3$ (BFN), $\text{CaCu}_3\text{Ti}_4\text{O}_{12}$ (CCTO), and NiO based ceramics [3–6] are some of the non-ferroelectric materials, which possesses excellent dielectric properties. These materials possess colossal dielectric constants (CDCs) of the order $>10^4$ in the vicinity of room temperature. In contrast to CCTO, BFN system is less studied. There is also a doubt about the relaxor ferroelectric nature of BFN system [7]. Further, there is

no evidence about the presence of permanent lattice dipoles in these CDCs materials. The origin of high dielectric constant in these non-ferroelectric systems is attributed to both intrinsic as well as extrinsic relaxations (grain boundary, electrode interface) effect near room temperature (RT) [8–10]. The sources of conduction and relaxation mechanisms in these materials are discussed in terms of *defect structures*. Movement of the presence charged point defects, free charge carriers, oxygen vacancies with temperature or the applied electric field in these materials contribute to the overall dielectric loss. Accumulation of charge carriers at the grain boundaries or at the electrode-material interface enhances the dielectric constant in these materials. The presence of transition metals, having more than one oxidation state like iron in BFN (Fe^{2+} and Fe^{3+}), in parent compound can act as charged point defect and facilitate hopping conduction. Extrinsic effects such as the electrode-material interface or grain-grain boundary interface, participate in Maxwell-Wagner (MW) relaxation or interfacial polarization, which contribute to the dielectric constant [7].

In the present work, in order to study and interpret the high dielectric constant near room temperature and the increase in dielectric constant with temperature in BFN system, the dielectric relaxation processes are investigated. The space charge model is used to explain the origin of high dielectric constant in BFN system [11]. Since M^* (complex electric modulus) plays simi-

* Corresponding author: tel: +91-0661-2462726
fax: +91-0661-2462926, e-mails: pawankumar@nitrkl.ac.in,
pvn77@rediffmail.com, pvn772004@yahoo.co.in

lar type of mechanism as that of ϵ^* (complex permittivity), the simultaneous study of both these complex impedance parameters may be helpful in the explanation for the involved processes.

II. Experimental details

Ba(Fe_{0.5}Nb_{0.5})O₃ ceramic samples were prepared by using solid state reaction route. Stoichiometric proportions of BaCO₃, Fe₂O₃ and Nb₂O₅ (all Merck India with >99% purity) were used as the starting initial reagents. The oxide powder was thoroughly mixed with acetone and ball milled for 12 h using zirconia balls. Calcinations were carried out at 1250 °C for 4 h. X-ray powder diffractometer (PHILIPS, PW 3020) was used for calcined powder diffraction pattern analysis. The calcined powder was grounded and mixed with 3 wt.% PVA (polyvinyl alcohol) as binder. Then the ceramic powder was uniaxially pressed at 90 MPa in the form of discs of diameter ~10 mm and thickness ~1 mm. These ceramic discs were sintered at 1350 °C for 4 h. The microstructure and surface morphology were analysed by using scanning electron microscope (JEOL SEM 6480LV). The sintered pellets were electroded using silver paste. The dielectric properties measurements as a function of frequency (100 Hz–1 MHz) and in the temperature range from the room temperature to 400 °C were carried out by using LCR meter (HIOKI 3532-50).

III. Results and discussion

3.1 Structural and microstructural analysis

The X-ray diffraction (XRD) pattern of the calcined powder is shown in Fig. 1. It can be seen from the XRD pattern that single perovskite phase is formed at 1250 °C for 4 h calcinations conditions. Lattice parameters with crystal structure are determined from the XRD pattern by using the least-squares method of a standard computer program (POWD) [12]. The best agreement between observed (*obs*) and calculated (*cal*) inter planar spacing d (i.e. $\sum \Delta d = \sum (d_{obs} - d_{cal}) = \text{minimum}$) is found for the cubic structure with $a = 4.0607 \text{ \AA}$. There is no change in phase composition after sintering of the titled ceramic.

Figure 2 shows the SEM image of BFN ceramics sintered at 1350 °C for 4 h. Dense microstructure with inhomogeneous grain size distribution can be seen in the SEM image. A non-uniform distribution of grains with grain size between 1–5 μm is observed.

3.2 Dielectric study

Figure 3 shows the variation of dielectric constant (ϵ') with temperature at different frequencies with temperature. The dielectric constant at different frequencies increases with the increase in temperature, and at frequency of 1 kHz it is ~17422, 108353 and 52655 at room temperature, 320 and 400 °C, respectively. In ϵ' versus temperature plot, the T_m (temperature at which ϵ' is maximum) decreases gradually with the increase

of frequency and a maximal dielectric dispersion occurs near T_m . This dielectric behaviour is different from those of relaxor ferroelectric materials. This hints that the BFN system is not a relaxor ferroelectric system. It is also confirmed from XRD study that the BFN ceramics are showing centro-symmetric nature of crystal symmetry at room temperature, which is a characteristic

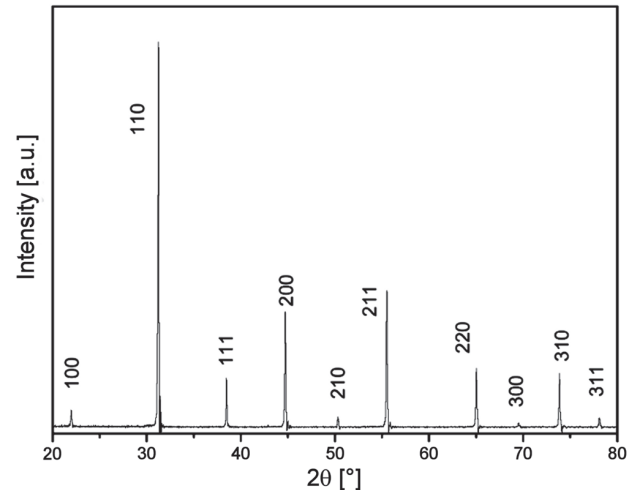


Figure 1. XRD pattern of BFN powder calcined at 1250 °C

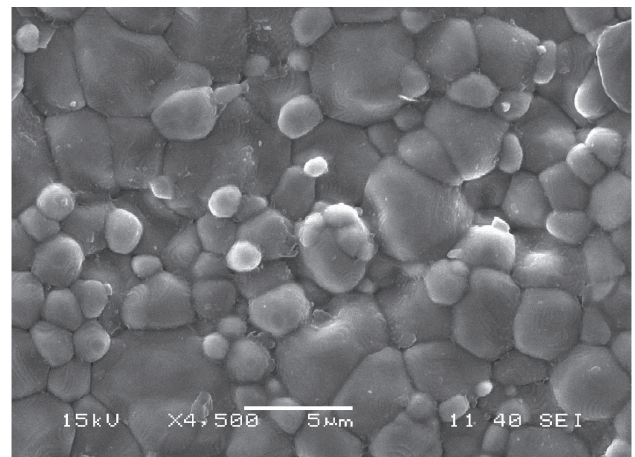


Figure 2. SEM of BFN ceramic sintered at 1350 °C

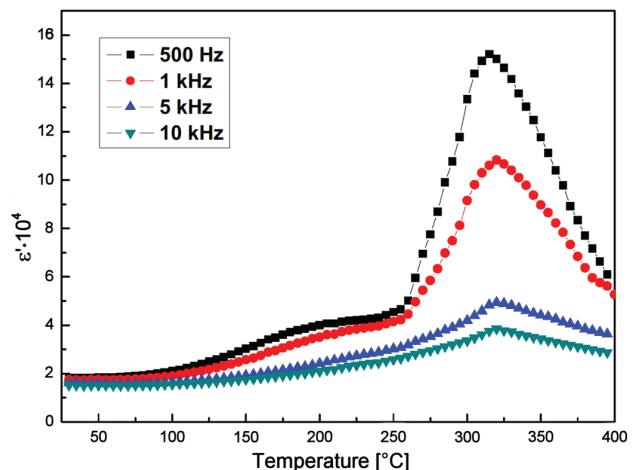


Figure 3. Variation of dielectric constant with temperature

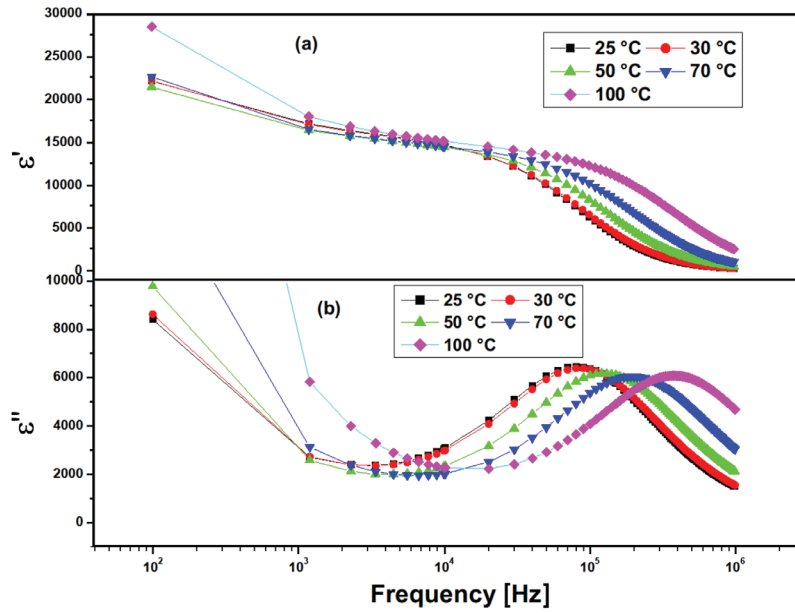


Figure 4. Variation of dielectric constant (ϵ') (a) and dielectric loss (ϵ'') (b) with frequency

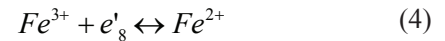
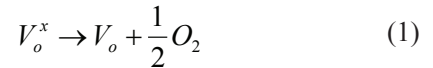
of non-ferroelectric materials. Further, in order to confirm the origin of dielectric behaviour in BFN ceramics, complex form of permittivity and modulus study is carried out.

Figure 4a,b show the variation of relative dielectric constant (ϵ') and dielectric loss (ϵ'') vs. frequency respectively in the temperature range RT to 100 °C. In the ϵ' spectroscopic plot, at low frequency, dielectric constant plateau is followed by a relaxation step. The high dielectric constant at low frequency is due to space charge effect. At higher frequency space charges weakly follow the varying AC field and hence a relaxation step is observed with decrease in dielectric constant. Corresponding to each relaxation step in ϵ' spectrum a dielectric relaxation peak is observed in ϵ'' spectroscopic plot. The characteristic peak, observed in ϵ'' spectrum, shift to higher frequency side with rise in temperature, this indicates that more than one relaxation phenomena are present in the sample. The asymmetric broadening of the relaxation peak suggests that there is an existence of distribution of relaxation time inside the material [13].

The complex conductivity ($\sigma^*(\omega) = \sigma_1(\omega) + j\sigma_2(\omega)$) directly relates to complex permittivity ($\epsilon^* = \epsilon' - j\epsilon''$). Experimental conductivity data are usually represented as real part ($\sigma_1(\omega)$) of frequency dependent complex conductivity ($\sigma^*(\omega)$). The real part of conductivity contributes to the imaginary part of permittivity and vice versa. It is advantageous to study the imaginary part of complex permittivity in order to distinguish the ionic conductivity from the polarization relaxation in the frequency space.

In order to explain the high dielectric constant and conduction process in BFN ceramics defect mechanism is considered. Formation of oxygen vacancies during high temperature sintering is a common result in all

types of oxide based perovskite materials. However, the amount of oxygen loss and its effect on the conduction process in different materials is different. These are expressed as Kröger-Vink notation as follows:



where V_o^x , V_o^\bullet , $V_o^{\bullet\bullet}$ are neutral, singly ionized and doubly ionized oxygen vacancies, respectively. Generally, the conduction process takes place by the movement of ionized oxygen vacancies or by the transport of free electron. As electrons are highly mobile with respect to single ionized and doubly ionized oxygen vacancies, room temperature conduction or relaxation mechanisms are mostly related to the free electrons. The electrons released during the process of ionization of oxygen vacancies process are trapped by Fe^{3+} ions, which becomes Fe^{2+} ions. This thermally activated process enhances the conductivity of ceramics. As both Fe^{2+} and Fe^{3+} ions simultaneously exist on the same crystallographic sites in BFN system, therefore there is a possibility of conduction by hopping mechanism.

Pure dielectric relaxation is more significant at cryogenic temperature range whereas the long range conduction processes are observed far away from room temperature. With increase in temperature, density of thermal energy assisted mobile charge carriers increases, which enhances the DC conductivity. The DC conductivity has considerable value at room temperature.

The dielectric loss in the samples can be described as due to either the DC and AC conductivity or dipole relaxation. The low frequency tail region in the $\text{Im}[\epsilon^*(\omega)]$ part represent the static conductivity, which can be easily separated from the high frequency relaxation (absorption peak) process. Whereas, the large capacitance of grain boundary or electrode interface polarizations contributes to the $\text{Re}[\epsilon^*(\omega)]$, thereby making it difficult to separate the pure relaxation part [14]. The complex permittivity can be described with modified Cole-Cole equation associating the conductivity term [15,16]:

$$\epsilon^* = \epsilon_\infty + (\epsilon_0 - \epsilon_\infty) / [1 + (j\omega\tau)^{1-\alpha}] + \sigma^* / (j\epsilon_0\omega^s) \quad (5)$$

where, σ^* is the complex conductivity, ϵ_0 is static permittivity, ϵ_∞ is the permittivity at high frequency, τ is the mean relaxation time and α is the angle inclination of the semicircular arc with the abscissa. The real and imaginary part of ϵ^* can be written as:

$$\epsilon'(\omega) = \epsilon_\infty + \frac{\Delta\epsilon}{2} \left(1 - \frac{\sinh \beta z}{\cosh \beta z + \cos \beta\pi/2} \right) + \frac{\sigma_2}{\epsilon_0\omega^s} \quad (6)$$

$$\epsilon''(\omega) = \frac{\Delta\epsilon}{2} \left(1 - \frac{\sin \beta\pi/2}{\cosh \beta z + \cos \beta\pi/2} \right) + \frac{\sigma_1}{\epsilon_0\omega^s} \quad (7)$$

where $z = \ln(\omega\tau)$, $\Delta\epsilon = \epsilon_0 - \epsilon_\infty$, $\beta = 1 - \alpha$ and τ is relaxation time period. For purely ohmic conduction $s = 1$. The conductivity (σ_1) due to free charge carriers (DC conductivity) contributes to $\text{Im}[\epsilon^*]$ and that of (σ_2) due to the space charges (localized charges) contributes to $\text{Re}[\epsilon^*]$. The first part of $\text{Im}[\epsilon^*]$ involves pure relaxation whereas the second part or the conductivity part involves long range conductivity [17]. The peak maxima of the ϵ'' spectrum satisfies the relation $\omega_{max}\tau = 1$. The obtained relaxation time period (τ) follows the temperature dependent Arrhenius law:

$$\tau = \tau_0 \exp(E_a / k_B T) \quad (8)$$

where τ_0 is pre-exponential factor, E_a is the relaxation activation energy, k_B is Boltzmann constant, and T is the absolute temperature. Using eqn. 8, the relaxation activation energy ($E_a = 0.19$ eV) and relaxation time at infinite temperature ($\tau_0 = 1.13 \cdot 10^{-9}$ s) are calculated from the linear plot shown in Fig. 5. The inset figure (in Fig. 5) shows nonlinear fit of imaginary part of permittivity at 60 °C.

The activation energy determined from dielectric relaxation in the temperature range RT to 100 °C is 0.19eV, which is nearer the activation energy (0.1eV) of the first ionization of oxygen vacancy [18]. This indicates that the electrons, released during the first ionization process, are directly trapped by the Fe^{3+} ions. In order to state the origin of relaxation and “giant” permittivity in BFN ceramics, the space charge model is described.

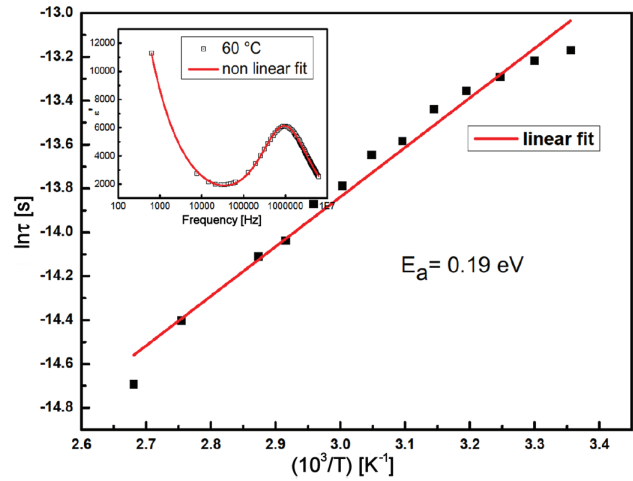


Figure 5. Variation of relaxation time period with temperature. Inset figure shows nonlinear fit of the frequency dependent dielectric loss (ϵ'') at 60 °C

3.3 Space charge model

The space charge model is used to explain the origin of “giant” permittivity in BFN perovskite ceramics. The low frequency dielectric relaxation ($\omega \rightarrow 0$) and the long range ionic conductivity of charge carriers can have close relation. For this model, the material should possess a large density of oxygen vacancies during processing conditions. The space charge polarization is strongly influenced by lattice defects and bulk conductivity. In ferroelectric materials above the Curie temperature (T_c) these oxygen vacancies are no longer confined to their defect site of the unit cell but extended to the whole sample, performing ionic conduction in the material. Localization of these space charges at the inner face of the grains is responsible for the dielectric relaxation in the materials. Therefore, the low frequency dielectric relaxation observed in these ferroelectric materials above the Curie temperature is due to space charge effect. This is the space charge model used for explaining the dielectric relaxation in ferroelectric materials [11]. However, non-ferroelectric ceramics like BFN system materials showing giant permittivity near room temperature can also be explained on the basis of space charge model. For this, the material should possess space charges in the vicinity of room temperature.

Below room temperature, thermal fluctuations are low; hence free charges are localized to their defect sites and hopping type of conduction occurs among the residual iron/oxygen vacancies sites in sintered BFN ceramics. As the temperature increases, free charges can move throughout the sample. The space charge polarization occurs in these ceramics near room temperature (RT) with low activation energy (0.1 eV) [19]. This suggests that at RT in BFN system, there are more localization sites available at the grain boundaries, which promote space charge effect [19].

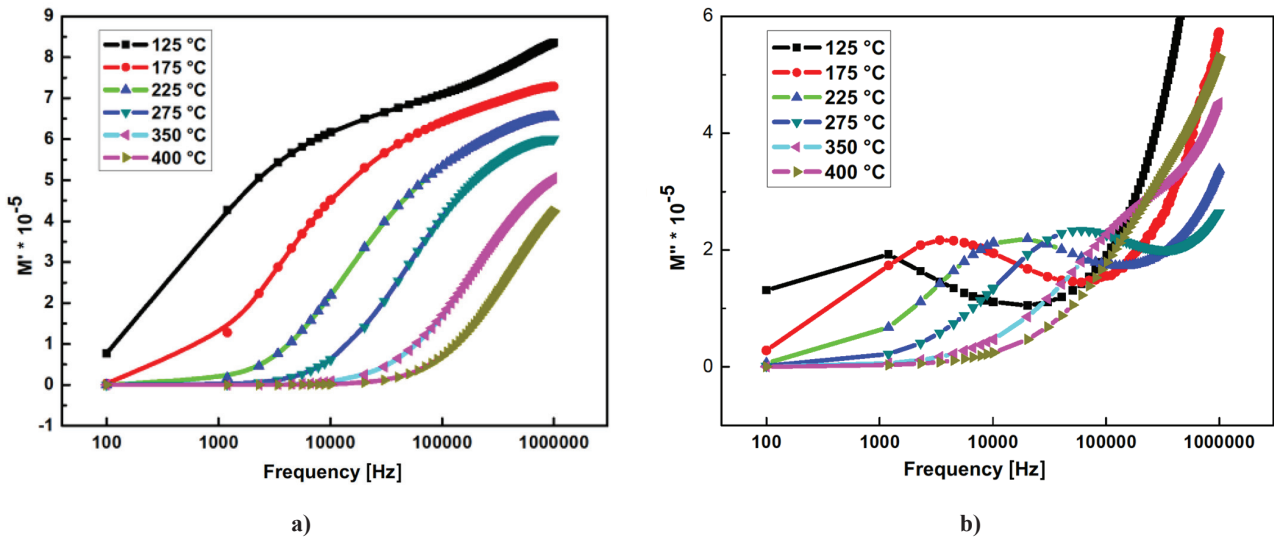


Figure 6. Variation of real (a) and imaginary part (b) of electric modulus with frequency at different indicated measurement temperatures

The charged point defects (V_{ρ}), formed at higher sintering temperature, become fixed to the ionic site of the unit cell when the samples are cooled down to room temperature. These ionized electrons take part in conduction process near room temperature. Accumulation of these charge carriers at the inner boundaries of grain, increase the overall dielectric permittivity. Here the grain boundary act as thin capacitor and the accumulated charges at the interfaces acts as electrodes for these capacitors, which helps in increasing the dielectric permittivity of the BFN ceramics. Also, the low value of activation energy (0.19 eV) fits well with the microscopic Maxwell-Wagner relaxation [19]. Hence, the giant dielectric constant of BFN ceramics near room temperature of BFN ceramics is due to microscopic effect of MW relaxation called as space charge polarization. The space charge model is fitted well with our result near room temperature.

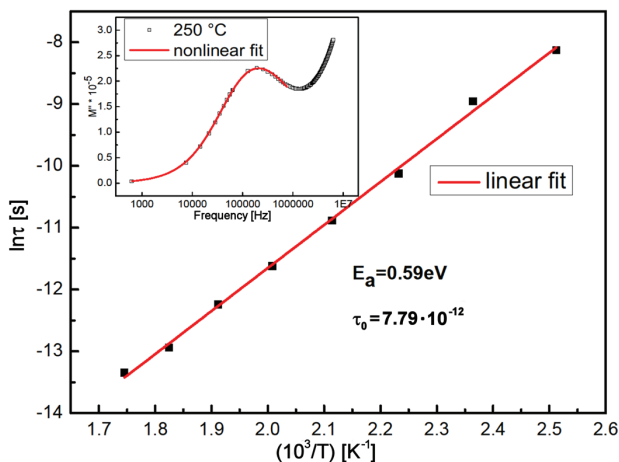


Figure 7. Variation of relaxation time period with temperature obtained from fitting the imaginary part of modulus. Inset figure shows non-linear fit of imaginary part of modulus at 250 °C

3.4 Modulus study

The electric modulus M^* is given by the inverse of complex dielectric permittivity and can be expressed in the following form [20]:

$$M^*(\omega) = 1 / \epsilon^*(\omega) = M'(\omega) + M''(\omega) \quad (9)$$

where $M' = \epsilon' / (\epsilon'^2 + \epsilon''^2)$ and $M'' = \epsilon'' / (\epsilon'^2 + \epsilon''^2)$ are real and imaginary part of complex modulus, respectively. The M' and M'' vs. frequency at different temperatures are plotted in Figs. 6a and 6b, respectively. The relaxation peak in M'' spectrum is not observed in the low temperature region (< 100 °C) whereas it starts appearing above 100 °C. This may be due to the fact that the chosen range of frequency (100 Hz to 1 MHz) is lower than the range in which the M'' relaxation peak falls or the range in which the relaxation ratio ($r = \epsilon_0 / \epsilon_{\infty}$, where ϵ_0 and ϵ_{∞} are dielectric constant at low and high frequency respectively) increases [21]. In the M'' versus frequency spectrum two relaxation peaks can be expected corresponding to grain and grain boundary effects, respectively. One relaxation peak appears in low frequency region due to the contribution from grain boundaries, while the other appearing in high frequency region is due to the contribution from grains. Both these relaxation peaks in a sample will appear provided that the capacitance of grains and grain boundaries are nearly the same [22]. As, $M'' = \epsilon_0 / 2C$; which means peaks corresponding to the large capacitance are diminished in the M'' plot. Therefore, the relaxation peak corresponding to electrode interface, which has larger capacitances, is suppressed in the M'' vs. frequency plot. As shown in Fig. 6b, the grain and grain boundary relaxations can be observed in the high and low frequency regions, respectively. The incomplete relaxation peak appears at higher frequency in M'' spectroscopic plot, which is due to the fact that the range of frequency chosen is not sufficient

for this process to be observed. The characteristic peak maxima of M'' spectroscopic plot obey the relation $\omega_{max} \tau = 1$. The low frequency data is fitted by using the following formula [23,24]:

$$M''(\omega) = \frac{M''_{max}}{(1-\beta) + \left(\frac{\beta}{1+\beta}\right) \left[\beta \left(\frac{\omega_{max}}{\omega}\right) + \left(\frac{\omega}{\omega_{max}}\right)^\beta \right]} \quad (10)$$

The obtained relaxation time τ ($= 1/\omega_{max}$) at different temperatures follows temperature dependent Arrhenius law (eqn. 8). The activation energy obtained from linear fit (Fig. 7) is ~ 0.59 eV and $\tau_0 = 1.7 \times 10^{-12}$. This value is closer (0.7 eV) to that of second ionization from oxygen vacancy V_o'' [25]. Therefore, it can be concluded that the oxygen vacancies mainly play important role in different types of relaxation processes and origin of giant dielectric constant in BFN systems. The inset figure (Fig. 7) shows nonlinear fit of frequency dependent imaginary part of modulus at 250 °C.

3.5 Space Charge Model at High Temperature

At higher temperature (>100 °C) electrons released from doubly ionized oxygen vacancy move towards the grain boundary. In polycrystalline materials grain boundaries play significant roles in their electrical properties. A Schottky barrier can be formed at the grain boundaries. The interfacial or Maxwell-Wagner polarization arises from Schottky barrier. Large activation energy (0.59 eV) is required for such interfacial polarization.

IV. Conclusions

Dielectric relaxation was studied in a wide temperature range. The relaxation activation energy was 0.19 eV and 0.59 eV in low and high temperature range calculated from permittivity and modulus formalism, respectively. Near room temperature (< 100 °C) and above 100 °C free electrons released from first-ionization and second ionization of oxygen vacancies were seen to take part in the respective relaxation processes. The experimental data fitted well for explaining the space charge model for the origin of high dielectric constant near room temperature in BFN system.

References

1. N. Setter, R. Waser, "Electroceramic materials", *Acta Mater.*, **48** [1] (2000) 151–178.
2. S.M. Spearing, "Materials issues in microelectromechanical systems (MEMS)", *Acta Mater.*, **48** [1] (2000) 179–196.
3. S. Saha, T.P. Sinha, "Low-temperature scaling behavior of $\text{BaFe}_{0.5}\text{Nb}_{0.5}\text{O}_3$ ", *Phys. Rev. B: Condens. Matter*, **65** [13] (2002) 134103.
4. A.P. Ramirez, M.A. Subramanian, M. Gardel, G. Blumberg, D. Li, T. Vogt, S.M. Shapiro, "Giant dielectric constant response in a copper-titanate", *Solid State Commun.*, **115** [5] (2000) 217–220.
5. M.A. Subramanian, D. Li, N. Duan, B.A. Reisner, A.W. Sleight, "High dielectric constant in $\text{ACu}_3\text{Ti}_4\text{O}_{12}$ and $\text{ACu}_3\text{Ti}_3\text{FeO}_{12}$ phases", *J. Solid State Chem.*, **151** [2] (2000) 323–325.
6. J. Wu, C.-W. Nan, Y. Lin, Y. Deng, "Giant dielectric permittivity observed in Li and Ti doped NiO", *Phys. Rev. Lett.*, **89** [21] (2002) 217601.
7. I.P. Raevski, S.A. Prosandeev, A.S. Bogatin, M.A. Malitskaya, L. Jastrabik, "High dielectric permittivity in $\text{AFe}_{1/2}\text{B}_{1/2}\text{O}_3$ nonferroelectric perovskite ceramics (A = Ba, Sr, Ca; B = Nb, Ta, Sb)", *J. Appl. Phys.*, **93** [7] (2003) 4130–4136.
8. D.C. Sinclair, T.B. Adams, F.D. Morrison, A.R. West, " $\text{CaCu}_3\text{Ti}_4\text{O}_{12}$: One-step internal barrier layer capacitor", *Appl. Phys. Lett.*, **80** [12] (2002) 2153–2155.
9. G. Deng, P. Murali, "On origin and intrinsic electrical properties of the colossal dielectric constant state in $\text{CaCu}_3\text{Ti}_4\text{O}_{12}$ ", pp. 012016 in: *IOP Conf. Ser.: Mater. Sci. Eng.*, Vol. 8, IOP Publishing, 2010.
10. P. Lunkenheimer, R. Fichtl, S.G. Ebbinghaus, A. Loidl, "Nonintrinsic origin of the colossal dielectric constants in $\text{CaCu}_3\text{Ti}_4\text{O}_{12}$ ", *Phys. Rev. B: Condens. Matter*, **70** [17] (2004) 172102.
11. O. Bidault, P. Goux, M. Kchikech, M. Belkaoumi, M. Maglione, "Space-charge relaxation in perovskites", *Phys. Rev. B: Condens. Matter*, **49** [12] (1994) 7868–7873.
12. E. Wu, "POWD, an interactive program for powder diffraction data interpretation and indexing", *J. Appl. Crystallogr.*, **22** [5] (1989) 506–510.
13. D.K. Mahato, A. Dutta, T.P. Sinha, "Dielectric relaxation in double perovskite oxide, $\text{Ho}_2\text{CdTiO}_6$ ", *Bull. Mater. Sci.*, **34** [3] (2011) 455–462.
14. K.L. Ngai, R.W. Rendell, "Interpreting the real part of the dielectric permittivity contributed by mobile ions in ionically conducting materials", *Phys. Rev. B: Condens. Matter*, **61** [14] (2000) 9393–9398.
15. K.S. Cole, R.H. Cole, "Dispersion and absorption in dielectrics I. Alternating current characteristics", *J. Chem. Phys.*, **9** [4] (1941) 341–351.
16. G. Georgoussis, A. Kanapitsas, P. Pissis, Y.V. Savelyev, V.Y. Veselov, E.G. Privalko, "Structure-property relationships in segmented polyurethanes with metal chelates in the main chain", *Eur. Polym. J.*, **36** (2000) 1113–1126.
17. T. Prasit, T. Suwat, Y. Teerapon, M. Santi, "Dielectric relaxation and dielectric response mechanism in (Li,Ti)-doped NiO ceramics", *J. Phys.: Condens. Matter*, **20** [39] (2008) 395227.
18. J. Daniels, K.H. Hardtl, "Electrical conductivity at high temperatures of donor-doped barium titanate ceramics", *Philips Res. Rep.*, **31** (1976) 489–504.
19. M. Maglione, "Polarons, free charge localisation and effective dielectric permittivity in oxides", pp. 3719 in *arXiv e-prints*: 1006.3719, 2010.
20. J.R. Macdonald, "Impedance spectroscopy", *Ann. Biomed. Eng.*, **20** [3] (1992) 289–305.
21. R. Gerhardt, "Impedance and dielectric spectroscopy revisited: Distinguishing localized relaxation from long-range conductivity", *J. Phys. Chem. Solids*, **55** [12] (1994) 1491–1506.

22. D.C. Sinclair, A.R. West, “Impedance and modulus spectroscopy of semiconducting BaTiO₃ showing positive temperature coefficient of resistance”, *J. Appl. Phys.*, **66** [8] (1989) 3850–3856.
23. R. Bergman, “General susceptibility functions for relaxations in disordered systems”, *J. Appl. Phys.*, **88** [3] (2000) 1356–1365.
24. C.R. Mariappan, G. Govindaraj, S.V. Rathan, G.V. Prakash, “Vitrification of K₃M₂P₃O₁₂ (M = B, Al, Bi) NASICON-type materials and electrical relaxation studies”, *Mater. Sci. Eng., B*, **123** [1] (2005) 63–68.
25. S.A. Long, R.N. Blumenthal, “Ti-rich nonstoichiometric BaTiO₃: II, Analysis of defect structure”, *J. Am. Ceram. Soc.*, **54** [11] (1971) 577–583.

